Investigations on one-way coupling effects of particle-laden decaying isotropic turbulent flows

Julian Stemmermann, Steffen Trienekens, Christian Soika

Aachen, 3rd of July 2017

Contents

1 Nomenclature

η	Kolomogorov scale
$\boldsymbol{\tau}$	Stress tensor
$\boldsymbol{I}$	Identity tensor
$\boldsymbol{S}$	Rate-of-strain-tensor
μ	Dynamic viscosity
ρ	Density
ρ_{p}	Particle density
$\tau_m athrmp$	Particle response time
$\boldsymbol{\nabla}$	Nabla-operator
$\boldsymbol{a}$	particle acceleration
$\boldsymbol{H^i}$	Stores the inviscid variables in the flux-vector included in the Navier-Stokes equations
$\boldsymbol{H^v}$	Stores the viscous variables in the flux-vector included in the Navier-Stokes equations
$\boldsymbol{H}$	Container for fluctuating variables in the Navier-Stokes equations
$\boldsymbol{Q}$	Container for conserved variables in the Navier-Stokes equations
$\boldsymbol{q}$	Heat conduction

$\boldsymbol{u}$	Three-dimensional velocity
$\boldsymbol{v_{\mathrm{p}}}$	Particle velocity
$\boldsymbol{v}$	particle velocity
$\boldsymbol{x_{\mathrm{p}}}$	Particle position
$\boldsymbol{x}$	particle position
c_p	Specific isobaric heat capacity
c_v	Specific isochoric heat capacity
E	Specific inner energy
e	Specific internal energy
$f_m athrmD$	Drag correction
k_t	thermal conductivity
m_{c}	number of clustered particles
p	Pressure
Pr	Prandtl number
R	Universal gas constant
r_p	Particle radius
Re	Reynolds number
S	Sutherland temperature
T	Temperature

2 Introduction

in Computational Methods for Multiphase Flow ist auf den Seiten 3-9 ein interessantes Beispiel. Sollen wir hier außerdem noch ein Bild von einer turbulenten Strömung und der Sammlung der Partikel in low-vortex-areas einfügen? Unterschiedliche Sections erklären Einführung von m_c beschreiben.

3 Mathematical models

Zusammenfassung mathematische Modelle und kurze Einleitung in das mathematische Grundkonzept der Simulation.

3.1 Single-phase flow

In this section the mathematical basics for understanding and simulating turbulent flows are discussed. However, it should be pointed out that this is no complete treatise of the mathematical and physical basics. The reader can achieve further insight on this topic by looking at different books and papers, e.g. [8].

3.1.1 The Navier-Stokes equations

The Navier-Stokes-Equations are of great importance for understanding turbulent phenomena. This set of equations exists in forms for compressible and incompressible fluids. For an infinitesimal small volume element $d\tau$ and using the cartesian coordinate system, they can be written in the so-called 'divergence form':

$$\frac{\partial \boldsymbol{Q}}{\partial t} + \boldsymbol{\nabla} \boldsymbol{H} = 0 \tag{3.1}$$

It should be noted by the reader that this work only contains investigations about chemically inert fluids and particles, and that the simulation results only fit under this condition. The vector $\boldsymbol{Q}$ contains all the variables which are conserved, i.e. the density ρ, the velocity $\boldsymbol{u}$ and the specific inner energy E:

$$\boldsymbol{Q} = \begin{pmatrix} \rho \\ \rho \boldsymbol{u} \\ \rho E \end{pmatrix} \tag{3.2}$$

$\boldsymbol{H}$ is the flux vector which stores all the floating variables and may be split up into two parts:

$$\boldsymbol{H} = \boldsymbol{H}^{\mathbf{i}} + \boldsymbol{H}^{\mathbf{v}} \tag{3.3}$$

The contents of the two vectors are displayed below:

$$\boldsymbol{H}^{\mathbf{i}} = \begin{pmatrix} \rho \boldsymbol{u} \\ \rho \boldsymbol{u} \boldsymbol{u} + p \\ \boldsymbol{u}(\rho E + p) \end{pmatrix} \tag{3.4}$$

5

$$\boldsymbol{H^{v}} = -\frac{1}{Re} \begin{pmatrix} 0 \\ \boldsymbol{\tau} \\ \boldsymbol{\tau u} + \boldsymbol{q} \end{pmatrix} \tag{3.5}$$

$\boldsymbol{H^{i}}$ is called inviscid flux and contains only the variables that are independent of the fluids viscosity, it describes the way a fluid with zero viscosity would behave. In contrast, the viscous flux $\boldsymbol{H^{v}}$ represents the effects of viscosity. The Reynolds number $Re = \frac{\rho v d}{\eta}$ is defined to be the ratio of inertia to tenacity, which makes it very valuable for understanding turbulent flows. This is also due to the fact that two familiar objects with the same Reynolds number behave similar in turbulence. One can assume that flows with $Re << 1$ are laminar and flows with $Re >> 1$ are turbulent. To solve the Navier-Stokes-Equations, more information regarding some variables is required. For Calculating the specific inner Energy E and the heat conduction $\boldsymbol{q}$, the following equations are used:

$$E = e\frac{1}{2}|\boldsymbol{u}|^2 \tag{3.6}$$

$$\boldsymbol{q} = -\frac{\mu}{Pr(\gamma-1)}\boldsymbol{\nabla}T \tag{3.7}$$

with

$$\gamma = \frac{c_p}{c_v} \tag{3.8}$$

and the Prandtl number

$$Pr = \frac{\mu_\infty c_p}{k_t} \tag{3.9}$$

using the specific heat capacities of the fluid c_v and c_p. If one could assume that the fluid is a newtonian fluid, the linear correlation between stress and the rate of strain results in:

$$\boldsymbol{\tau} = 2\mu\boldsymbol{S} - \frac{2}{3}\mu(\boldsymbol{\nabla} * \boldsymbol{u})\boldsymbol{I} \tag{3.10}$$

in which $\boldsymbol{S} = \frac{(\boldsymbol{\nabla u})(\boldsymbol{\nabla u})^T}{2}$ denotes the rate-of-strain-tensor. Additionally, the viscosity μ can be aprroximated through Sutherland's law, which is based on the ideal gas-theory:

$$\mu(T) = \mu_\infty(\frac{T}{t_\infty})^{3/2}\frac{T_\infty + S}{T + S} \tag{3.11}$$

S is in this case the Sutherland temperature. To achieve closure the caloric state equation $e = c_v T$ and the state eqaution for an ideal gas $p = \rho RT$ are used. The specific gas constant is determined by $R = c_p - c_v$. These equations form a set of partial differential equations, so for solving them starting values are needed.

3.2 Particle dynamics

Siewert: -3.1a-3.14 (spherical particles) OHNE GRAVITATION Stokes Drag/Stokes Coefficient Filterung (Fritz) -¿Viskositaet durch numerischen Fehler, Smagorinksy nicht benutzen

Cause this work deals with particle laden fluids and the impact of these particles on the flow conditions, we need to describe the interaction between them. We deal with small and heavy, rigid particles, that have a spherical shape. Their radius r_p is even smaller than the Kolmogorov scale η, but also large enough to neglect the Brownian motion. Due to the small particle concentration, the best and most common way to describe these flows is the point particle approach, which means that every particle is treated as an mathematical point source of mass, momentum and energy. In this case we focus on the momentum exchange.Effects like particle-particle interactions, particle-wall interactions are also neglected. At describing the motion of the particles in the following the fact, that we deal with gas-solid flows is an advantage, since we can make several simplifications. First we look at the influence of the particles on the carrier fluid. Here we make the assumption, that the fluid is incompressible and the mass exchange over the particle surface is zero. Hence the continuity equation becomes:

$$dreieck * \boldsymbol{u} \tag{3.12}$$

. The Navier Stokes equation, described in chapter 1, becomes:

$$\rho * (-F) \tag{3.13}$$

The influence of the particles on the fluid is represented by the new term F, wich describes the force per unit volume on the fluid. We could approximate F by a superposition of Dirac's delta functions over all particles, centered at the location x_p^n of each particle:

$$F = f^n \tag{3.14}$$

$\boldsymbol{x_p^n}$ is the position of the n-th particle and results from the kinematic equation

$$\frac{\partial \boldsymbol{x_p}}{\partial t} = \boldsymbol{v_p} \tag{3.15}$$

$\boldsymbol{v_p}$ is the velocity of the n-th particle. $\boldsymbol{f^n}$ is the sum of forces acting between fluid an particles. Hence it plays also an important role in the equation of motion of the particles:

$$v_v * \rho_p * \frac{\partial \boldsymbol{v_p^n}}{\partial t} = v_v * \rho_p * \boldsymbol{g} + \boldsymbol{f^n}(\boldsymbol{x_p^n}) \tag{3.16}$$

As already mentioned $\boldsymbol{f^n}(\boldsymbol{x_p^n})$ could be devided in several forces. Then the equation of motion looks like:

$$v_v * \rho_p * \frac{\partial \boldsymbol{v_p^n}}{\partial t} = v_v * \rho_p * \boldsymbol{g} + \boldsymbol{f_d} + \boldsymbol{f_l} + \boldsymbol{f_a} + \boldsymbol{f_h} + \boldsymbol{f_{additional}} \qquad (3.17)$$

Here $\boldsymbol{f_d}$ represents the hydrodynamical drag force that is parallel to the undisturbed streamlines, which depends on an empirical drag coefficient C_d:

$$\boldsymbol{f_d} = -\frac{3}{4} * \rho * v_v * \frac{C_d}{d} * |\boldsymbol{v_p} - \boldsymbol{u}| * (\boldsymbol{v_p} - u) \qquad (3.18)$$

$\boldsymbol{u}$ is the velocity of the uniform stream, which is enough away from the particle that it is undisturbed from the particle. The other partial hydrodynamical force, the lift force $\boldsymbol{f_l}$ is perpendicular to the undisturbed streamlines. Furthermore the added mass force $\boldsymbol{f_a}$ represents the influence of the inertia of the fluid that has an impact on the particle, if it has a different acceleration than the mean flow. Hence it could be determined by:

$$\boldsymbol{f_a} = \frac{1}{2} * \rho * v_v * \left(\frac{D * \boldsymbol{u}}{D * t} - \frac{d * \boldsymbol{v_p}}{d * t} \right) \qquad (3.19)$$

———-nie $\boldsymbol{v}$ sondern immer $\boldsymbol{v_p}$ benutzen——— The history force $\boldsymbol{f_h}$ takes diffusion and convection, that results out of the vortices behind the particles, into account. We look at Basselt's result, neglecting the finite size correction that is proportional to $\boldsymbol{\nabla}^2 * \boldsymbol{u}$:

$$\boldsymbol{f_h} = \frac{3}{2} * d^2 * \rho * \sqrt{\pi * \nu} * \int_t 0^t \frac{dt'}{(t - t')^{1/2}} \left(\frac{D\boldsymbol{u}}{Dt'} - \frac{d\boldsymbol{v_p}}{dt'} \right) \qquad (3.20)$$

In our case of gas-solid suspensions we can make several simplifications. In the following we show with an rough approximation that the added mass and history forces are negligible compared with the drag force. We use the approach that the relative velocity is of the same order as the terminal velocity v_t. The terminal velocity is the velocity of a particle in a resting fluid, when gravitation and drag force are in equilibrium. Then if the added mass and the drag force are compared, we get the following equation:

$$\frac{|\boldsymbol{f_a}|}{|\boldsymbol{f_d}|} \simeq\approx \frac{\frac{1}{2} * \rho * v_v * g}{\frac{3}{4} * \rho * v_v * (C_d/d) * v_t^2} \frac{a_r}{g} = \frac{1}{2} * \frac{\rho}{\rho_p} * \frac{a_r}{g} \qquad (3.21)$$

with

$$a_r = \left(\frac{D\boldsymbol{u}}{dt} - \frac{d\boldsymbol{v_p}}{dt} \right) \qquad (3.22)$$

8

Since in gas-solid suspensions the particle density is of an factor of 1000 higher than the fluid density, it shows that, if it's not the unlikely case that the relative acceleration is of the same order higher than the gravity, the added mass force is negligible compared to the drag force. The effect that fluid and particle influence each other is called two-way-coupling. $\boldsymbol{f_\mathrm{d}}$ and lift forces, $\boldsymbol{f_\mathrm{a}}$ the added mass and $\boldsymbol{f_\mathrm{h}}$ the history forces. The last term $\boldsymbol{f_\mathrm{additional}}$ is attached for the case that we have to take other forces like electrostatic interactions into account.

-coupling Zahl

The relaxation time τ_p physically represents the time scale over which the drag force decreases the particle relative velocity to zero and is determined by the following equation:

$$\tau_\mathrm{p} = \frac{rho_\mathrm{p}}{rho} * \frac{2 * r_\mathrm{p}^2}{9 * \nu} \tag{3.23}$$

Since we consider gas-solid flows, wich means we can use a point particle approach make some simplificantions in the following To get a usefull equation of motion for the particles in the flow, we use the Euler Lagrangian approach, as it is common in Direct Numerical Simulations (DNS) and Large Eddy Simulations (LES). The density of the particles ρ_p is much higher than that of the fluid ρ_f . In addition due to the very low particle concentration we can neglect the influence of the particles on each other. That means that the cross each other without any effect. That means particle collision is neglected. After all this simplifications we obtain a simplified version of the Maxey-Riley equations.

$$\frac{\partial \boldsymbol{x_\mathrm{p}}}{\partial t} = \boldsymbol{v_\mathrm{p}} \tag{3.24}$$

$$\frac{\partial \boldsymbol{v_\mathrm{p}}}{\partial t} = \frac{f_mathrmD}{tau_mathrmp}(\boldsymbol{u}(\boldsymbol{x_\mathrm{p}}) - \boldsymbol{v_\mathrm{p}}) \tag{3.25}$$

$\tau_mathrmp$ is the particle response time and a factor to obtain the drag force in Stokes flow conditions. To take the case of an Reynolds number $\Re$ of order 1 into account the correction factor $f_D = 1 + 0.15 Re_p^(0.687)$ is used. The biggest simplification of this Lagrangian approach is that the interaction of particles coming close together is neglected.

4 Numerical methods

To simulate flows like those described above we have two options. The direct numerical simulation (DNS) is the easier one to understand, although it is numerically very expensive. The Large-eddy simulation (LES) is numerically more capable, still we must accept certain inaccuracies. These two numerical methods are now discussed in the following chapter.

4.1 Direct numerical simulation

The basis of the direct numerical simulation (DNS) are the Navier-Stokes equations as described above. The idea is that the computer is very good at calculating and solves these equations completely. This provides a very accurate result, as all scales of motion are being resolved. Still it requires an immense level of comptational resources which increases rapidly with the Reynolds number. These computational resources were not available until the 1970s. Even though it is not advisable to resolve every scale of motion, if only the contained energy is of greatest interest. With the large-eddy simulation, as described below, the comptational effort is 99.98 % less compared to DNS, which indeed is the fraction of the dissipative scale. This leaves 0.02 % of the flow, which is correlative with the fraction of the energy-containing larger-scale [8].

4.2 Large-eddy simulation

Due to the fact that DNS is effortful and wasting resources if a fully resolved resolution is not required, large-eddy simulation (LES) was created to save time and resources. This is especially efficient if mainly the temproal energy trend is considered, because the energy containing larger-scale motion is completely resolved and the indeed small effects of the expensive smaller-scale motion are just modelled. Otherwise in DNS resolving the small dissipative scale would require most of the computational resources.
Simulating only the larger-scale motions is also called filtering, which means that the smaller-scale motions are filtered out. To model the filtered smaller-scale motions ususaly a subgrid-scale (SGS) model is used. According to Hickel (2007) the interference between explicit SGS and the truncation error can be exploited, i.e. the truncation error can serve as model of the effects of unresolved scales, which is therefore an implicit SGS model. Thus we call it implicit LES (ILES) [5].

4.3 Discretisation

To integrate the Lagrangian particle tracking equations, discussed above, a predictor-corrector scheme based on the trapezoidal rule for numerical integration

$$f(t + \delta t) \approx f(t) + \frac{\delta t}{2} \left[\frac{\partial f(t)}{\partial t} + \frac{\partial f(t + \delta t)}{\partial t} \right] \tag{4.1}$$

is used.

The first step is the prediction of the new particle position $\boldsymbol{x}_{n+1}^{(\mathrm{p})}$ using a Taylor expansion for a small time step δt

$$\boldsymbol{x}_{n+1}^{(\mathrm{p})} = \boldsymbol{x}_n + \delta t \boldsymbol{v}_n + \frac{1}{2} \delta t^2 \boldsymbol{a}_n. \tag{4.2}$$

Due to the computational effort we will put $\boldsymbol{u}_{n+1}^{(\mathrm{p})}$ on the level of the nearest cell fluid velocity.

The updated velocity and acceleration are calculated as

$$\boldsymbol{v}_{n+1} = \frac{\boldsymbol{v}_n + \frac{1}{2} \delta t \left(\boldsymbol{a}_n + \frac{f_{\mathrm{D}}}{\tau_{\mathrm{p}}} \boldsymbol{u}_{n+1}^{(\mathrm{p})} + \boldsymbol{g} \right)}{1 + \frac{1}{2} \frac{f_{\mathrm{D}}}{\tau_{\mathrm{p}}} \delta t}, \tag{4.3}$$

$$\boldsymbol{a}_{n+1} = \frac{\frac{f_{\mathrm{D}}}{\tau_{\mathrm{p}}} \left(\boldsymbol{u}_{n+1}^{(\mathrm{p})} - \boldsymbol{v}_n - \frac{1}{2} \delta t \boldsymbol{a}_n \right) + \boldsymbol{g}}{1 + \frac{1}{2} \frac{f_{\mathrm{D}}}{\tau_{\mathrm{p}}} \delta t}. \tag{4.4}$$

The updated particle position must be corrected by an additional term according to the trapezoidal rule

$$\boldsymbol{x}_{n+1} = \boldsymbol{x}_n + \frac{1}{2} \delta t \left(\boldsymbol{v}_{n+1} + \boldsymbol{v}_n \right) + \frac{1}{12} \delta t^2 \left(\boldsymbol{a}_{n+1} - \boldsymbol{a}_n \right). \tag{4.5}$$

4.4 Particle clustering

The high number of point particles require even more computational resources for the particle-laden simulation. The main idea to reduce this requirement is to create clusters of point particles, meaning that a new variable m_{c} is introduced. We consider a cluster of m_{c} point particles as one larger point particle, i.e. the program has less particles to simulate. To compensate this lack of particles, the coupling force is multiplied by m_{c}, due to the m_{c}-fold mass of the (cluster-)particles. In chapter 5 (results) we evaluate the legitimacy of particle clustering and the maximum acceptable value of m_{c}.

Projektion (noComputationalParticles), Diskretisierung implizite LES (Motivation fuer LES - Pope Chapter 9, Bild 9.4), DNS

5 Results

The simulations where carried out using ZFS, the simulation tool developed and implemented at the Institute of Aerodynamics at RWTH Aachen University [1] [2]. The tool is capable of simulating finite-volume flows of compressible fluids. In this case the turbulence was simulated on a cubic grid using 64^3, 96^3, 128^3 and 256^3. The first three cases where simulated using LES, the case in which 256^3 cells where used is carried out as DNS. Futher information can be gained by looking at [8, p.344-357 for DNS and p. 558-639 for LES].

For simplification, the special case of isotropic turbulence was used. For this idealised flow form the statistical velocities are invariant in all directions of the grid. It follows that the flows velocity are invariant for rotations and reflections. The turbulence was initialised using a seed-based random generator. To achieve physical results, the simulation of the particle-free flow was carried out to timestep 150, at which a restart file was written out. This procedure ensures a fully developed turbulent flow, whom has emancipated from the initialisation. In this flow field, a specific number of spherical particles were injected.

As noted in [6], particles tend to cluster in certain regions of the turbulent flow. This behavior can bee used to minimize computational effort for simulating the flow while still achieving high quality results. To investigate the differences in accuracy for different sizes of particles sizes, the variable m_c was introduced to the code describing the number of particles in one cluster. The simulations where then set up with the overall same number of particles (10^6), just the number of particles in one cluster was altered. Then the simulations where carried out normally and result in the following graphs (Figure 1, 2 and 3). It can be seen in figure 1 that the decay in kinetic energy from the starting point depends in a degree that is not negligible for most applications. With 10 particles per cluster, the solutions could be usable to get a first impression for technical purposes, all other simulations show a very high variety.

Fitting to this first results, the Graphs of figure 2 and 3 clearly show that for simulations with highly clustered particles the simulations are not very accurate. Looking at the results for the change in kinetic Energy, the difference becomes evident: The lower m_c is, the higher is the drop in kinetic Energy. This behavior can be seen because of the particles initially 'soaking up' energy, then in later phases of the flow giving it back in form of their inertia and speed, which they gathered in the beginning. **This effect should grow bigger by particle size and weight.** This change in energy transfer occurs at the unclustered simulation at about one eddy turnover time (t^*).
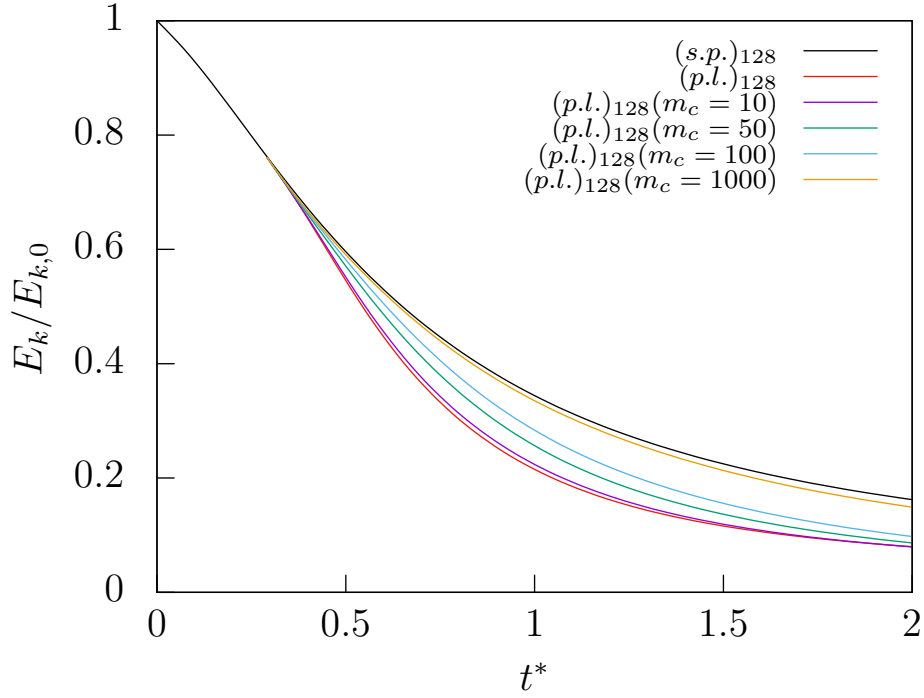
12

Figure 1: Kinetic Energy over time

In cases with more clustered particles it occurs later, only the case in which 1000 particles where clustered shows a strange behavior. It catches up the particle-free case very fast, which leads to the conclusion that the amount of clusters is so small that the flow almost behaves like one without particles. Additional the change in kinetic Energy shows inconstancy which can also be traced back to the small cluster number. The amount is just to small to achieve high-quality information in the statistical variables.

The same impression can be achieved by looking at the graphs describing the coupling rate. The particle-laden-case makes the biggest jump into negative coupling rate, which is defined as: **Defnition Coupling Rate**. The higher the amount of coupled particles, the lower is the negative coupling force. This evolution continues until the physicality vanishes and the randomness starts to show at the results for m_c higher than 50.

One could conclude that particle clustering is one, but propably not the best method to minimize computational effort. It makes sense to a certain extent, but as one can see from the simulations, the boundaries show fast.

To find out at which number of particles the results are sufficiently exact, a second set of simulations was carried out. As mathematics of turbulent flows are based on averaged variables, small numbers of particles can lead to false
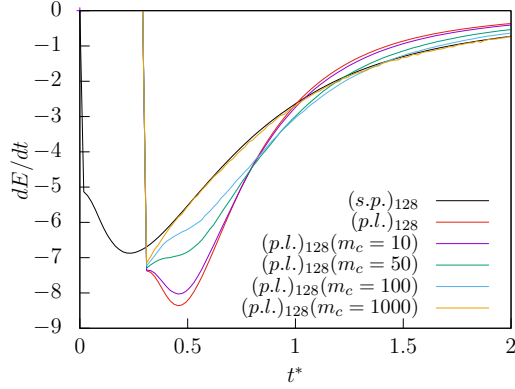
Figure 2: Change in kinetic Energy
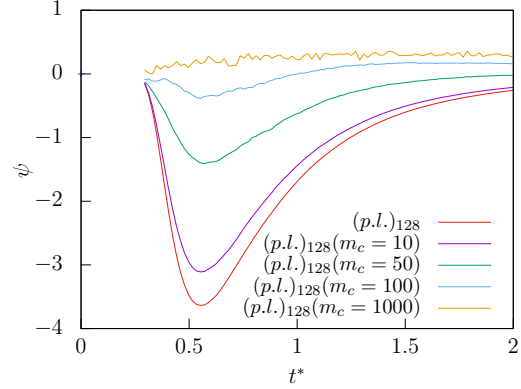over normalized time

Figure 3: Coupling Rate over
normalized time

and even unphysical results. In these simulations, no particle clustering was used, just different amount of particles where injected into the same flow. The results can be seen on page 15 on figure 4. The normalized difference in **kinetic Energy** shows as expected a clear correlation between particle number and accuracy in the simulation. Athough this was just a single initialization of particles in a flow, it can be stated that simulations using only 10^2, 10^3 or even up to 10^4 particles are not accurate enough for technical or scientific use of the data. Simulations in other gridsizes show similar results.
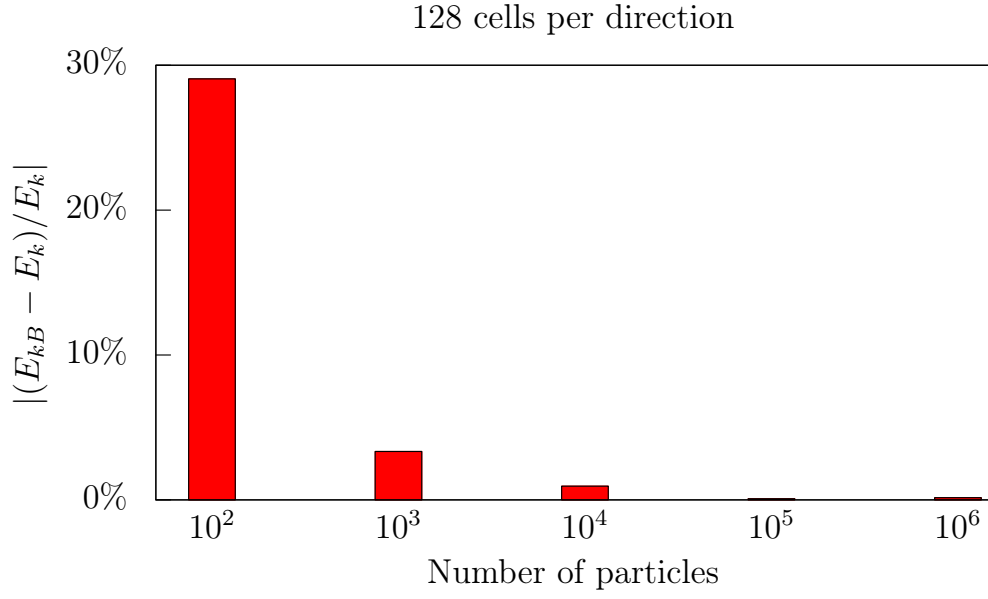
Figure 4: Results for initializing different numbers of particles

Case	Re	Re_λ	$Re_\lambda(restart)$	$c_f l$	timesteps	m_c	particle Diameter
64	?	?	?	?	?	?	?
96	?	?	?	?	?	?	?
128	?	?	?	?	?	?	?
264	?	?	?	?	?	?	?

Table 1: Example of a table

6   Conclusion

7 References

[1] W. Schröder D. Hartmann, M. Meinke. An adaptive multilevel multigrid formulation for cartesian hierarchical grid methods. *Comput. Fluids*, 2008.

[2] W. Schröder D. Hartmann, M. Meinke. A strictly conservative cartesian cut-cell method for compressible viscous flows on adaptive grids. *Comput. Meth. Appl. Mech. Eng.*, 2010.

[3] S. Elghobashi. Particle-laden turbulent flows: direct simulation and closure models. *Applied Scientific Research*, 1991.

[4] S. Fritz. Simulation isotroper turbulenz. study work, 2003.

[5] S. Hickel. *Implicit Turbulence Modeling for Large-Eddy Simulation*. PhD thesis, Technische Universität München, 2007.

[6] John K. Eaton John R. Fessler, Jonathan D. Kulick. Preferential concentration of heavy particles in a turbulent channel flow. *Physics of Fluids*, 1994.

[7] M. Meinke K. Fröhlich, L. Schneiders and W. Schröder. Validation of particle-laden large-eddy simulation using hpc systems. In *Sustained Simulation Performance 2017*, 2017. unpublished conference document.

[8] S. B. Pope. *Turbulent Flows*. Cambridge University Press, 2010.

[9] A. Prosperetti and G. Tryggvason. *Computational Methods for Multiphase Flow*. Cambridge University Press, 2009.

[10] W. Schröder. Fluidmechanik. lecture notes 'Fluid mechanics', 2010.

[11] C. Siewert. *Numerical Analysis of Particle Collisions in Isotropic Turbulence*. PhD thesis, RWTH Aachen University, 2014.